Pergamon

Int. J. Heat Mass Transfer. Vol. 41, Nos 4–5, pp. 797–808, 1998

Printed in Great Britain
0017-9310/98 $19.00+0.00

PII: S0017-9310(97)00130-0

A numerical study of natural convection immersion cooling of multiple heat sources in parallel interacting open-top cavities

M. BEHNIA and A. A. DEHGHAN
School of Mechanical and Manufacturing Engineering, The University of New South Wales, Sydney, Australia

and

H. MISHIMA and W. NAKAYAMA
Department of Mechanical and Intelligent Systems Engineering, Tokyo Institute of Technology, Tokyo, Japan

(*Received* 12 *April* 1996 *and in final form* 11 *April* 1997)

Abstract—Natural convection immersion cooling of two heat sources in a series of parallel interacting cavities filled with FC-72 has been numerically studied. Both low thermal conductivity (i.e. bakelite) and high thermal conductivity substrates (i.e. alumina–ceramic) have been considered. Comparison has been made between single and double heat source configurations. Non-dimensional temperatures and Nusselt numbers of the heat sources have been correlated as a function of the Rayleigh number. © 1997 Elsevier Science Ltd.

1. INTRODUCTION

Liquid cooling of microelectronic components has recently received considerable attention. Substantial improvement in heat removal capability, packaging and circuit density has been achieved by implementation of this cooling technique when compared with forced air cooling or indirectly water-cooled computers (i.e. thermal conduction module design). Liquids which are employed in immersion cooling must be chemically inert, non-toxic and have high dielectric properties. These features exclude the use of water as a coolant. The family of dielectric coolants known as Fluorinerts have such characteristics and are normally used in direct cooling techniques.

Natural convection immersion cooling is widely applicable for intermediate packaging level and surface heat fluxes ($10^3 < q''[\mathrm{W\,m^{-2}}] < 10^4$). It provides reliable, low cost and maintenance-free cooling [1]. Furthermore, information gained from natural convection immersion cooling can provide a platform under which nucleate boiling begins as noted by Bergles and Bar-Cohen [2].

The advantages of passive immersion cooling have prompted many experimental and numerical investigations to determine the heat transfer performance from microelectronic components. Typical geometries such as microchips mounted on substrates and encapsulated or immersed in enclosures filled with coolants have been analyzed, e.g. Milanez and Bergles [3] experimentally investigated the buoyancy-induced flow arising from a line heat source and multiple heat sources mounted on a vertical wall. The results were presented for different values of heat flux ratio of two heat sources and their separation distance for both air and water and compared with the boundary layer solution of Jaluria [4]. The effect of the heater size and its configuration were the main objectives of the experimental study of Park and Bergles [5] in which natural convection immersion cooling of protruding heat sources mounted on a vertical substrate was considered. It was shown that the heat transfer coefficients of the discrete heaters are higher than the predicted values by conventional correlation of Fujii and Fujii [6]. For a two in-line heat source configuration, it was found that the ratio of heat transfer coefficient of the upper heat source to the lower one was always below unity and this ratio increased with increasing the separation distance between the two heaters. However, they observed that it approached an asymptotic value of 0.9, which is in contradiction with the experimental observation of Milanez and Bergles [3] and the theoretical results of Jaluria [4], where a continuous increase in this ratio was found with increasing the separation distance. For the case of protruding heat sources, Park and Bergles [5] concluded that the top heater always exhibited a greater heat transfer coefficient.

Keyhani *et al.* [7] experimentally investigated buoyancy-driven flow and heat transfer in a tall cavity with discrete heat sources on one vertical wall while the opposed vertical wall was uniformly cooled. Eleven

NOMENCLATURE

c_p	specific heat capacity
d	width of the cavity
f_{cond}	fraction of conduction to the walls at heat sources locations
g	the acceleration due to gravity
H	height of the cavity
k_r	thermal conductivity ratio, k_s/k_f
l	separation distance between the heat sources
Nu	Nusselt number, $-\{1/\theta_w(X)\}\{\partial\theta_w(X)/\partial Y\}$
p	vertical position of the heat source
Pr	Prandtl number, ν/α_f
q''	input heat flux (dimensional)
Ra^*	modified Rayleigh number, $(g\beta q'' d^4/k_f\nu^2)(Pr/\lambda)$
s	height of the heat source
t	time
T	temperature
U	dimensionless velocity in the x-direction, ud/α
V	dimensionless velocity in the y-direction, vd/α
w	thickness of the walls
w_r	wall thickness ratio, w/d
x and y	coordinates
X and Y	dimensionless coordinates, x/d and y/d.

Greek symbols

α	thermal diffusivity, $k/\rho c_p$
α_r	thermal diffusivity ratio, α_s/α_f
β	the coefficient of thermal expansion
ξ	dimensionless vorticity
θ	dimensionless temperature, $(T-T_0)/(q''d/k_f\lambda)$
λ	aspect ratio, H/d
ν	kinematic viscosity
ρ	density
τ	dimensionless time, t/d^2
Ψ	dimensionless stream function.

Subscripts

1,2	first (upper) and second (lower) heat source
f	fluid
0	ambient condition
s	solid
w	surface of the wall.

equally-spaced constant heat flux flush-mounted heated strips were placed on a vertical adiabatic wall. Keyhani *et al.* [8] extended their previous investigation by employing a cavity with a smaller aspect ratio and three equally-spaced flush-mounted heat sources attached to the adiabatic vertical wall of a cavity with an aspect ratio of 4.5. It was concluded that the information obtained from the experiments with ethylene glycol can be applied for dielectric fluids, as they provide nearly the same heat transfer data. The same configuration was considered in the numerical study of Shen *et al.* [9] in order to determine the effect of heater size and aspect ratio on the heat transfer performance of the heat sources and flow patterns.

Natural convection from a protruded heat generating source mounted on a conductive substrate and immersed in a liquid-filled enclosure was studied by Sathe and Joshi [10]. They also found that increasing or decreasing the ratio of thermal conductivity of the solid to fluid beyond some limiting values had a marginal effect on the maximum temperature. Immersion cooling on a microelectronic chip encapsulated in a package was the subject of the experimental study of Joshi and Paje [11]. The package was mounted in a vertical substrate which was one of the vertical walls of a cubical enclosure. Both horizontal and vertical orientations of the package substrate assembly were considered. Sathe and Joshi [12] extended their previous work to study natural convection from substrate-mounted protrusions in a liquid-filled square enclosure, and considered the effects of Prandtl number protrusion thermal conductivity, protrusion width and substrate height on the flow and temperature fields and on the maximum protrusion temperature. The effects of different boundary conditions on the wall of the enclosures were also examined. A drop in the maximum temperature of between 14 and 18% was achieved when the protrusion width was increased. Wroblewski and Joshi [13] numerically investigated the transient three-dimensional natural convection in a rectangular cavity with a leadless chip encapsulated within a ceramic package and passively cooled by FC-77. Their attention was focused on the transient nature of the flow and thermal fields. The transient behavior was divided into four stages, i.e. initial heat up process of the chip, symmetric heat spreading through the package and development of natural convection, followed by increased natural convection with maximum buoyant force and finally a gradual approach to the steady state. In their recent studies Wroblewski and Joshi [14, 15] were concerned with the final steady state results and considered the effect of different independent parameters like Rayleigh number (i.e. heat generation rate), substrate thermal conductivity, geometrical parameters and thermal boundary conditions. The heat conducted to the substrate was reduced by 14% by increasing the Rayleigh number from 10^3 to 10^6 due to a stronger

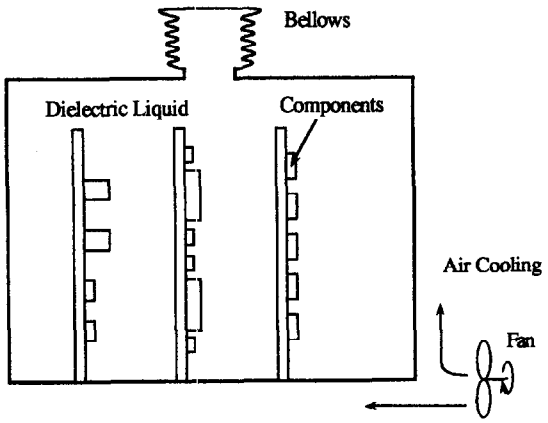

Fig. 1. Submerged immersion cooling module for electronic components.

convection. A decrease in the maximum temperature of 5–16% was achieved when the cold boundary was considered to be the top wall and front surfaces, respectively.

Most of these investigations considered a single vertical substrate containing the heat sources immersed in an enclosure or acted as one wall of the cavity. The interaction between heat sources mounted on a common substrate has received less attention. In more practical configurations, discretely heated vertical substrates are immersed in a large container and are orientated parallel to each other as noted by Bergles and Bar-Cohen [2]. The heat generated by micro-elements is convected away by the coolant and is later dissipated in an internal condenser or to the enclosure walls as shown in Fig. 1. In the present study, we consider a more realistic configuration of multiple interacting vertical slots. The walls have a finite thickness and thermal conductivity. On each wall there is one or two flush-mounted discrete heat sources with uniform heat flux (see Fig. 2). The vertical walls are assumed to be placed on the bottom of a large enclosure and interact with the ambient through the open top boundaries. From the literature, it appears that investigations on repeated channels are somewhat scarce. The numerical investigation of Kim *et al.* [16] is one of the limited number of studies in natural

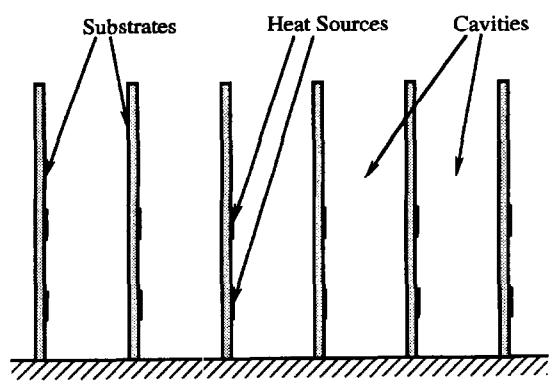

Fig. 2. Schematic diagram of the repeated cavities.

convection air cooling of parallel channels in which conducting walls with embedded line heat sources were considered. In their study, the heat sources are extended over the entire length of the heated side of the vertical walls, and heat dissipated to the walls was assumed to be entirely convected into the adjacent channel. However, heat generating devices are normally discretely distributed on a printed circuit board. Therefore, the portion of heat conducted to the vertical walls may either eventually be convected to the same channel upstream or downstream of the heat source, or dissipated by convection in the adjacent channel, thereby affecting its heat transfer performance.

The immersion cooling technique is normally applied to an array of highly integrated circuit cards (or boards). The most likely size of the card is 100 by 100 mm, as is seen in the multi-chip modules used in the mainframe computers today. These modules have a ceramic wiring card and the sintering process of the card dictates that dimension. Also, due to the requirements of a short wiring length on the card, the 100 mm size is considered as a practical limit. In general, the spacing between adjacent boards of the order of 20 mm (since it is close to 1 in). The 1 in. spacing has been an industry standard for many computers. In the future generation of immersion cooled computers a spacing of 2 mm may be a likely value.

The objective of this study is to numerically investigate the natural convection immersion cooling of multiple heat sources mounted in a series of cavities, as shown in Fig. 2. The closure of the bottom has the purpose of imposing the most hostile environment. In this study we intend to find the lower bound of the capability of immersion cooling and hence the bottom of the channel is assumed closed. The effects of heat flux and wall thermal conductivity on the heat transfer performance is determined. The interaction between the heat sources and between the adjacent cavities is also examined.

2. ANALYSIS

2.1. *Mathematical formulation*

The flow and thermal fields in a series of channels shown in Fig. 2 are almost the same except for the first and last channels which must be treated differently. Hence the computational domain is restricted to one of the middle channels as shown in Fig. 3.

The vorticity-stream function formulation of the Navier–Stokes equations is used in the fluid region. These equations are formulated for a laminar, two-dimensional and incompressible fluid, with constant properties except for the density in the buoyancy term of the momentum equation, which is assumed to follow the Boussinesq approximation. The two-dimensional model equations in non-dimensional form are as follows:

$$\frac{\partial \xi}{\partial \tau} + \frac{1}{Pr}\left(U\frac{\partial \xi}{\partial X} + V\frac{\partial \xi}{\partial X}\right) = \nabla^2 \xi + Ra^* \frac{\partial \theta}{\partial X} \quad (1)$$

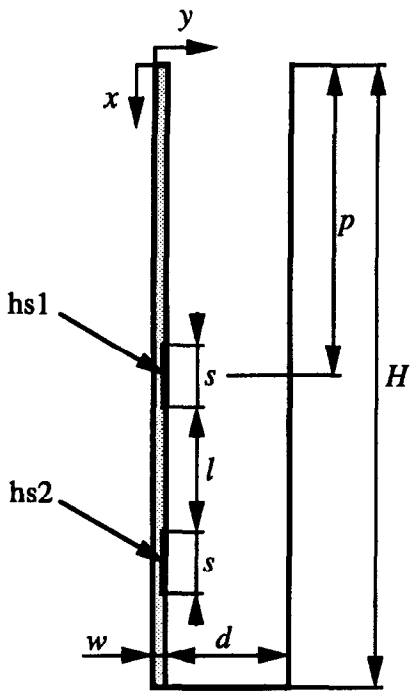

Fig. 3. Schematic diagram of the computational domain.

$$\frac{\partial\theta}{\partial\tau}+\frac{1}{Pr}\left(U\frac{\partial\theta}{\partial X}+V\frac{\partial\theta}{\partial X}\right)=\frac{1}{Pr}\nabla^2\theta \tag{2}$$

$$\nabla^2\Psi+\xi=0 \tag{3}$$

in which the non-dimensional variables U, V, τ and θ are defined as follows

$$U=ud/\alpha_f \tag{4}$$

$$V=vd/\alpha_f \tag{5}$$

$$\tau=\frac{tv}{d^2} \tag{6}$$

$$\theta=\frac{(T-T_0)k_f\lambda}{q''d}. \tag{7}$$

Stream function (Ψ) and vorticity (ξ) have their conventional definitions as follows:

$$U=\frac{\partial\Psi}{\partial Y},\quad V=-\frac{\partial\Psi}{\partial X} \tag{8}$$

$$\xi=\frac{\partial V}{\partial X}-\frac{\partial U}{\partial Y}. \tag{9}$$

In the solid region, the transient two-dimensional conduction equation is:

$$\frac{\partial\theta_s}{\partial\tau}=\frac{\alpha_r}{Pr}\left(\frac{\partial^2\theta_s}{\partial X^2}+\frac{\partial^2\theta_s}{\partial Y^2}\right). \tag{10}$$

The local Nusselt number along the vertical surfaces is defined as follows:

$$Nu(X)=-\frac{1}{\theta_w(X)}\frac{\partial\theta_w(X)}{\partial Y}. \tag{11}$$

2.2. *Boundary conditions*

All the solid walls are assumed to be impermeable, non-slip and stationary. The top and bottom ends of the vertical walls and the bottom wall of the cavity are assumed to be adiabatic. The temperature at any point on the hot and cold surfaces are unknown *a priori* and must be determined as a part of the solution procedure. An energy balance on the solid–fluid interface gives the following additional thermal boundary conditions:

$$k_r\left(\frac{\partial\theta}{\partial Y}\right)_s=\left(\frac{\partial\theta}{\partial Y}\right)_f+\lambda \quad \text{at the heat source locations} \tag{12}$$

$$k_r\left(\frac{\partial\theta}{\partial Y}\right)_s=\left(\frac{\partial\theta}{\partial Y}\right)_f \quad \text{at locations other than the heat sources} \tag{13}$$

in which $\lambda=H/d$.

The repeated nature of the slots requires that the temperature and heat flux at any point on a vertical wall is the same as those of other vertical walls at the corresponding location. This is true only for intermediate slots, whilst the first and the last channels behave differently. These boundary conditions are referred to as the repeated boundary conditions [16] and may be written as:

$$\theta_{(X,0)}=\theta_{(X,1+w/d)} \tag{14}$$

$$k_r\left(\frac{\partial\theta}{\partial Y}\right)_{(X,0)}=\left(\frac{\partial\theta}{\partial Y}\right)_{(X,1+w/d)}. \tag{15}$$

The computational domain is restricted to the cavity due to both computational economy and simplicity. Therefore, appropriate boundary conditions are required for the open top. Here it is assumed that the incoming fluid is at the ambient temperature (i.e. $\theta_{in}=0$), and the outgoing flow is assumed to have a zero axial temperature gradient (i.e. $\partial\theta/\partial X=0$). For the case of a single heat source mounted on a vertical wall, Jaluria [17] has shown that the flow is of a boundary layer type and downstream of the heat source this is a valid assumption, especially for higher Grashof numbers. The horizontal component of the velocity, V, is assumed to be zero at the open boundary. The boundary condition for the vertical velocity, U, is obtained from the continuity equation which gives $\partial U/\partial X=0$. The hydrodynamic boundary conditions at the open top when translated to the vorticity-stream function form, yields $\partial\Psi/\partial X=\partial\xi/\partial X=0$. In summary, the boundary conditions applied to the open boundary are as follows:

$$\theta_{in}=0 \quad \text{for incoming flow} \tag{16}$$

$$\left(\frac{\partial\theta}{\partial X}\right)_{\text{out}} = 0 \quad \text{for outgoing flow} \tag{17}$$

$$V = \frac{\partial U}{\partial X} = \frac{\partial \Psi}{\partial X} = \frac{\partial \xi}{\partial X} = 0 \quad \text{for both flows.} \tag{18}$$

The same approximate boundary conditions were used by Gosman *et al.* [18] in their numerical study of heat transfer within an open thermosyphon. For shallow open cavities Chan and Tien [19] showed numerically and experimentally that the basic flow pattern and heat transfer characteristic of the cavity can be adequately predicted by employing the approximate open boundary conditions described above. They also showed that even for square cavities at moderate to high Rayleigh numbers, the flow and heat transfer was identical with that obtained from extending the computational domain outside the cavities. Abib and Jaluria [20] employed the same boundary conditions as Gosman *et al.* [18] for predicting the buoyancy driven flow generated by a discrete isothermal heat source inside a partially open enclosure. More recently, Lage *et al.* [21] and Jones and Cai [22] adopted this approach and used the same boundary conditions which are used in this study in their numerical study of natural convection heat transfer from open top cavities.

2.3. *Numerical scheme*

If transient results are sought, equations (1), (2) and (10) can be discretized and solved by an alternative direction implicit (ADI) scheme which is well suited for solving parabolic partial differential equations. Iterative methods or a direct solver must be employed for solving the Poisson equation at each time step. However, since only the steady state solution is of interest in the present study, a pseudo-transient approach is adopted for solving the prescribed equations. A false time derivative is added to the right-hand side of equation (3) and all the equations are marched in time with different time steps. This will allow the use of an ADI scheme for all the equations. Therefore, at the expense of loss of the true transient solution, considerable saving in the computational effort is achieved. Furthermore, greater numerical stability and a faster rate of approach to the steady state solutions was achieved by using a power law scheme [23] for the differencing of the equations (1) and (2). The resulting discretized equations were solved by the Samarskii and Andreyev [24] ADI scheme. Application of this scheme results in a system of linear algebraic equations with a tridiagonal matrix in each direction, which can be solved by the Thomas algorithm.

3. RESULTS AND DISCUSSION

Examination of the governing equations (1)–(3) and (10) and interface boundary conditions (12)–(18) reveals that the independent parameters are Rayleigh number (Ra^*), Prandtl number (Pr), ratio of thermal conductivity of the wall to fluid (k_r), the ratio of the wall thickness to the cavity opening (w_r) and ratio of the cavity height to its width (λ). In the present work FC-72 is considered as the working fluid ($Pr = 12.4$). Calculations are performed for a fixed cavity opening and aspect ratio (i.e. $\lambda = 5$) corresponding to slots with 100 mm height, 20 mm width and 2 mm thick walls. The effects of the input heat flux (i.e. Ra^*) are examined for the range of Ra^* from 6.8×10^8 to 5.5×10^{10} which corresponds to a chip heat flux, q'', from about 1000–80 000 [W m^{-2}]. It is noted that in this range the flow was found to be steady, however, at higher Rayleigh numbers there will be a transition to unsteadiness. In this study both heat sources are assumed to generate the same heat flux ($q''1/q''2 = 1$). For comparison purposes, single heat source results are presented for cases where only the upper heat source (hs1) is active with an input heat flux of $q''1$. The locations of the heat sources (i.e. hs1 and hs2) are fixed and correspond to $2.25 < X < 2.75$ and $3.75 < X < 4.25$, respectively. This results in a separation distance between the heat sources (l/s) of 2. The effect of k_r is studied by varying k_r from 0 to 632 which covers adiabatic to alumina–ceramic walls. It is noted that for the adiabatic walls case the flow and thermal fields inside one slot are not affected by the others.

As there are no available immersion cooling experimental data pertinent to our geometry and conditions, the numerical model could not be directly validated for this case. However, for the case of a single heat source, experiments have been performed in air and there was good agreement with predictions as reported in Dehghan and Behnia [26]. We have also performed mesh sensitivity computations in order to obtain mesh independent results. It was found that a uniform mesh of 101×101 in the fluid and 5 mesh points in the solid region is adequate. Doubling of mesh points in both the fluid and solid only changed the average Nusselt number by less than 1%. Computations were performed on an IBM RISC/6000-320 workstation with approximately 40 CPU minutes required for 1000 iterations. Around 40 000–80 000 iterations were needed to obtain the steady state solution. The run time can be shortened by using the converged solution of a previous case as a starting solution. The convergence to steady state was checked by both a local monitoring of the dependent variables and applying an energy balance criterion.

For a fixed geometry and working fluid, Ra^* is proportional to the input heat flux. Figure 4 shows the predicted flow patterns and isotherms for $Ra^* = 6.82 \times 10^8$, 6.82×10^9 and 1.364×10^{10} and for $k_r = 24.6$ (bakelite substrate). The cold flow enters the cavity in the middle region of the opening and moves towards the closed end (this is the flow direction for all figures presented here). As the incoming flow moves towards the bottom of the cavity it loses its vertical

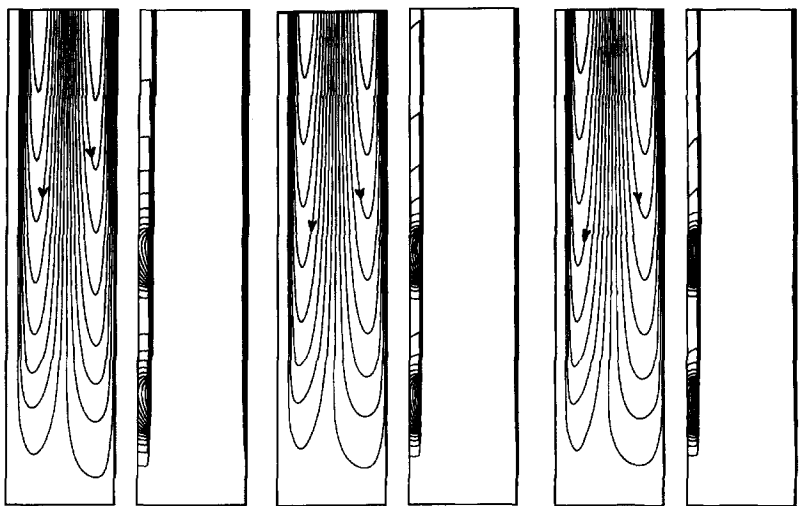

Fig. 4. Streamlines and isotherms for various Ra^* and $k_r = 24.6$: (a) $Ra^* = 6.82 \times 10^8$ [streamline contour levels: minimum = 2.6, increment = 2.6]; (b) 6.82×10^9 [min = 7.3, inc = 7.3]; and (c) 1.36×10^{10} [min = 10, inc = 10].

momentum. It then turns around and moves along both vertical walls towards the open boundary. The velocities are high along both walls with a low velocity flow in the rest of the cavity. The flow is nearly symmetrical for lower Ra^* and becomes non-symmetrical as the chip heat flux is increased. The isotherms reveal that a thin thermal boundary layer is formed along both walls. The rest of the cavity is occupied by the cold fluid. The thickness of the velocity boundary layers is larger than the thermal boundary layers due to the relatively high Pr. The upward flow outside of the thermal boundary layer is shear-driven. The isotherms in the solid region are concentrated in the vicinity of the heat sources and its density is higher for larger Ra^*. The same flow patterns were observed for the case of alumina–ceramic substrate with $k_r = 632$ (for sake of brevity the results are not shown here). The flow was asymmetrical with respect to the centerline of the cavity and the two thermal boundary layers along the cold (right) and hot (left) faces are almost identical. It is noted that in the cavity we refer to the substrate with chip as 'hot wall' and the one without it as 'cold wall' although neither of the walls is isothermal. The reason for the asymmetrical flow pattern is due to equal wall temperature on the hot and cold walls caused by the low thermal resistance in the substrate in Y-direction. The isotherms in the solid region are more evenly distributed in X-direction in comparison with the lower conductivity substrate (see Fig. 4) in which high temperature gradients are seen in the substrate around the heat sources. For low conductivity substrates, the thermal boundary layers begin to develop from around the leading edge of hs2, whilst for the higher conductivities, the starting point for the boundary layer is at the bottom of the walls.

Figure 5 presents the temperature distribution across the middle of the cavity at the center of hs1 for $k_r = 24.6$. The interface between the solid and fluid regions is shown by a dotted line. The temperature distribution in the solid region is almost linear. It is seen that thin boundary layers exist along the cold and hot faces. It is obvious that the thickness of the boundary layers reduce with increasing Ra^*. For the case of smaller Ra^*, weaker buoyancy of the fluid—which is heated by hs2 and upstream wall locations—induces a smaller rising fluid velocity, and a longer time is needed for the fluid to reach to the position of hs1. Hence, thermal diffusion in the fluid in Y-direction is more pronounced for the case of lower Ra^* which results in a thicker thermal boundary layer. This in turn causes a thicker area of generating buoyancy and hence a thicker hydrodynamic boundary layer. The fluid rising on the colder face has a lower temperature and hence a lower buoyancy compared to the fluid adjacent to the hot face causing a flow asymmetry as was seen in Fig. 4. Examination of the same profile for $k_r = 632$ revealed that the profiles were almost symmetrical with respect to the centerline of the cavity.

Figure 6 shows the non-dimensional temperature distribution on the hot and cold faces of the walls, which are faces corresponding to the heat source side and the opposite side, respectively, for two values of Ra^* and $k_r = 24.6$. The non-dimensional temperatures are smaller for higher values of Ra^*. This is due to the definition that θ is inversely proportional to the chip heat flux. For both Ra^*, temperature distributions show a rapid variation around the leading and trailing edges of the heat sources, with the maximum local temperatures on the heat source locations. The differences between the temperature of

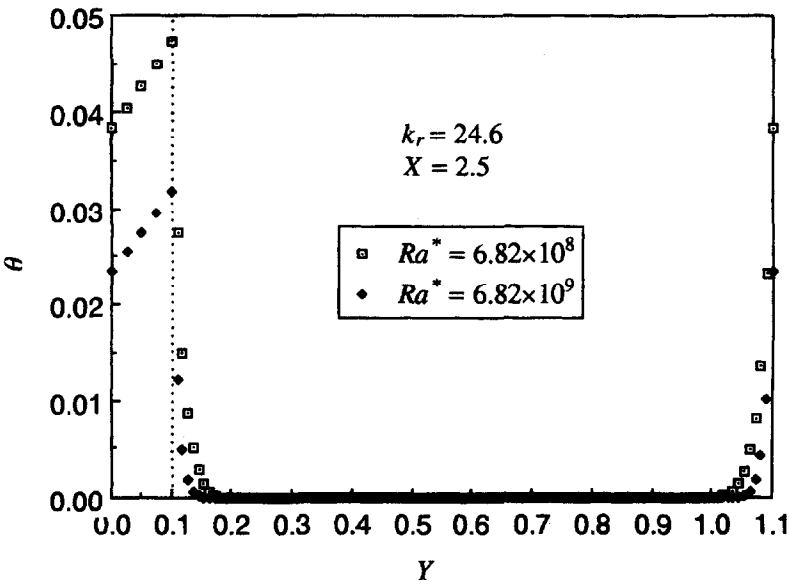

Fig. 5. Temperature distribution across the cavity at the mid-point of hs1 ($X = 2.5$) for $k_r = 24.6$ (two heat source configuration).

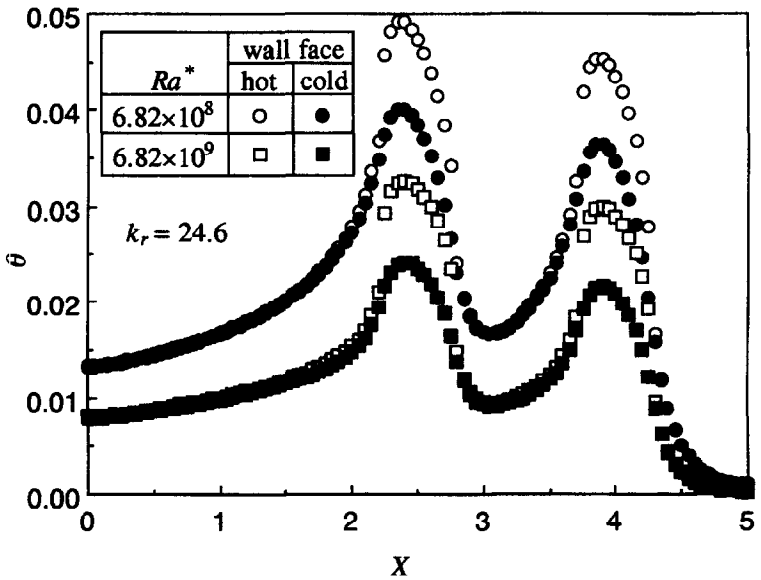

Fig. 6. Temperature distribution along the hot and cold faces of the vertical wall for $k_r = 24.6$.

the hot and cold faces are higher and these differences increase with increasing the chip heat flux. For instance, $\Delta T_{max} = 0.6$ K for $Ra^* = 6.82 \times 10^8$ and 5.9 K for $Ra^* = 6.82 \times 10^9$, hence, there is an increase in the flow asymmetry with a higher plume velocity along the hot wall as Ra^* increases (see Fig. 4). In the other locations along the walls, no appreciable temperature difference on the two sides are observed. The wall temperature is higher downstream of hs1 than upstream of the bottom source due to the thickening of the thermal boundary layer.

The temperature profiles for $k_r = 632$ (not shown here) indicated a smoother temperature variation for this case compared to Fig. 6. Temperature of the upstream section of hs2 was significantly increased compared to the case of $k_r = 24.6$. This is due to the lower thermal resistance in the substrate in the X-direction. No appreciable difference in the temperature difference between the hot and cold faces was observed. Hence a symmetric flow was obtained as described earlier.

Reliability considerations dictate that chip temperatures are maintained below a safe functional limit. Hence, one of the objectives of the thermal control analysis is to predict the chip temperature and printed circuit boards temperature distribution. Figure 7

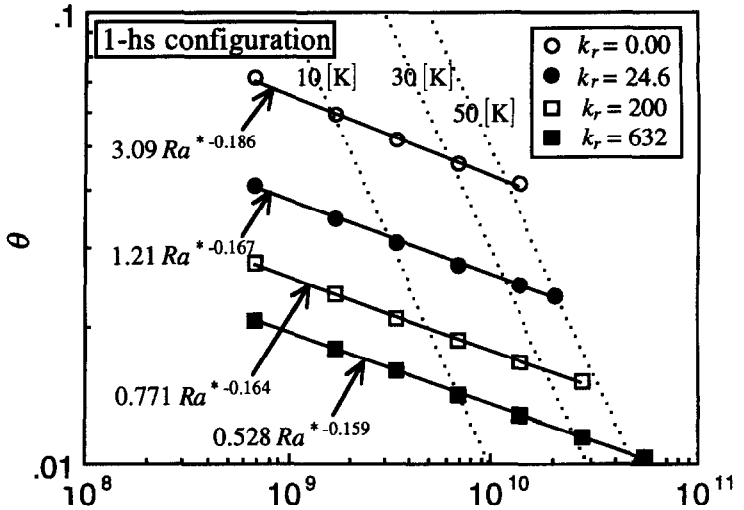

Fig. 7. Variation of non-dimensional heat source temperature with Ra^* for various k_r (single heat source configuration).

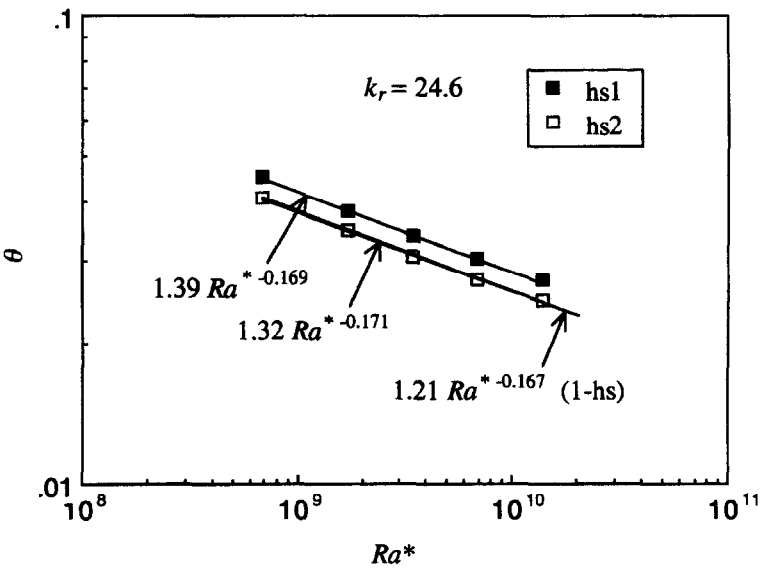

Fig. 8. Variation of non-dimensional temperature of the heat sources with Ra^* for $k_r = 24.6$ (two heat source configuration).

shows the variation of the average non-dimensional temperature of the heat source with Ra^* in the single heat source configuration (1-hs) for the base case ($k_r = 0$) and other values of k_r. The results are well correlated by straight lines; correlations between θ and Ra^* are derived for different k_rs. The exponent of Ra^* is negative for all cases. By its definition, θ_s represents the thermal resistance between the heat source and the ambient fluid. The thermal resistance is reduced by enhancement of convection, which is driven by a stronger buoyancy as Ra^* increases. Except for the case of $k_r = 0$, the exponents of Ra^* are found to be in a narrow range of around -0.163 (± 0.004). This means that, although the thermal resistance is higher for smaller k_r, the increase of heat source intensity produces almost an equal degree of enhancement of buoyancy-driven convection for all finite k_rs considered in this study, i.e. $24.6 < k_r < 632$. The dotted lines at Fig. 7 are traces of constant temperature difference between the heat source and the ambient fluid. The line of 50 K is a possible upper limit for single phase convection beyond which boiling begins. The drawing of this line is based on the estimation that, with an incoming fluid temperature of 15°C, the surface temperature reaches 65°C, high enough to trigger boiling of FC-72, which requires a few degrees of superheating above the boiling point (56°C) as reported by Heindel *et al.* [25]. It facilitates the estimation of maximum allowable heat source flux for single phase heat transfer; 3.14×10^4 and 6.84×10^4 W m^{-2} for $k_r = 24.6$ and 632, respectively.

The θ and Nu variations for two heat source configuration (2-hs) are shown in Figs 8 and 9, respectively, where the wall thermal conductivity is set at

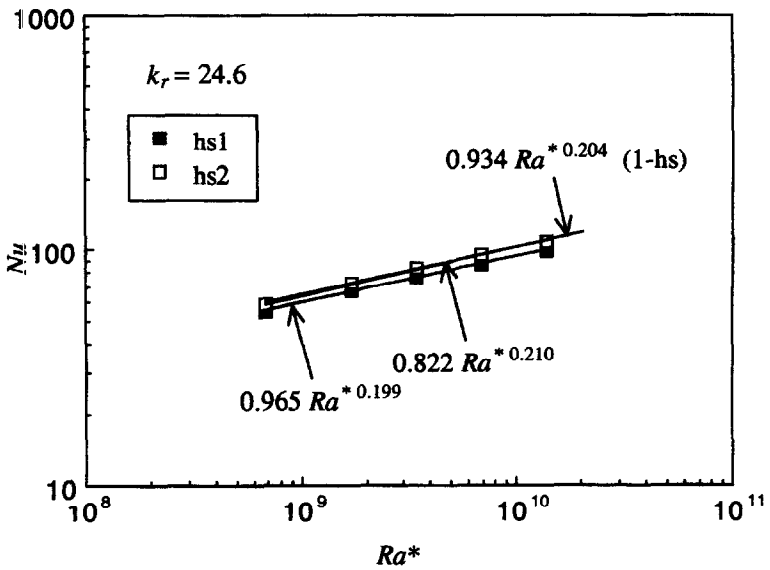

Fig. 9. Variation of Nu of the heat sources with Ra^* for $k_r = 24.6$ (two heat source configuration).

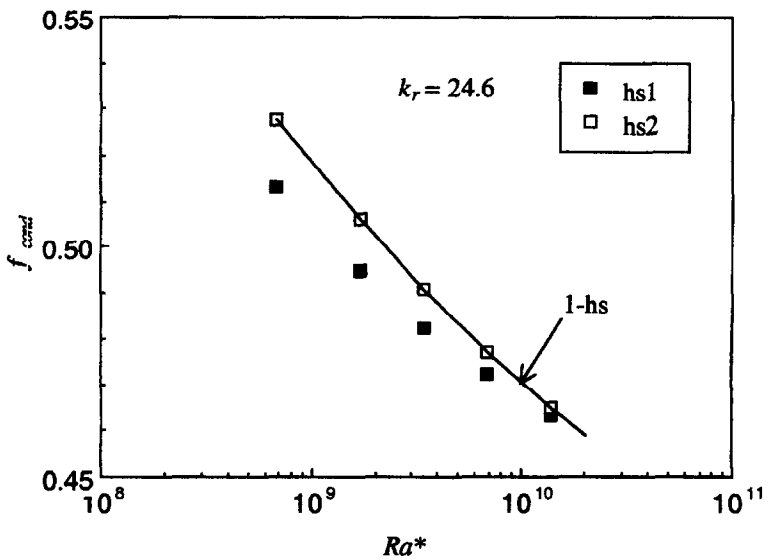

Fig. 10. Variation of conduction ratio (f_{cond}) with Ra^* for $k_r = 24.6$ (two heat source configuration).

$k_r = 24.6$. Note that Nu, defined by equation (11), is averaged on the heat source area. The correlations for the single heat source configuration (1-hs) are also shown for comparison. The results for the upper heat source (hs1) and the lower heat source (hs2) are well correlated by straight lines which are almost parallel to those for the case of 1-hs. Besides, the results for hs2 depart only marginally from those of 1-hs. This results from the fact that, for $k_r = 24.6$ and $l/s > 2$, the heat dissipation from hs1 has a negligible influence on the heat transfer performance of hs2. On the other hand, the temperature of hs1 is increased, thereby decreasing its Nu, when hs2 is introduced. This is due primarily to the effect of thermal wake from hs2 covering hs1, because conductive interaction in the substrate between the heat sources is negligible for this separation distance. For the range of Ra^* studied, an increase of around 10% in θ and a decrease of around 8% in Nu of hs1 are found when the lower heat source is introduced.

Due to the conjugate nature of the problem, both conduction to the substrate and convection to the fluid are responsible for the cooling of the microchips. The conductive heat transfer from the heat source to the substrate normalized by the heat generation from the source (f_{cond}) is presented in Fig. 10 for $k_r = 24.6$. The heat conduction to the substrate is partially convected to the neighboring cavity from the back surface, and the rest is convected from the front surface regions upstream and downstream of the heat sources. For both heat sources, f_{cond} reduces as Ra^* is increased, due to the stronger induced convection heat transfer from the heat sources. The f_{cond} values are larger for hs2 than hs1 and their difference diminishes

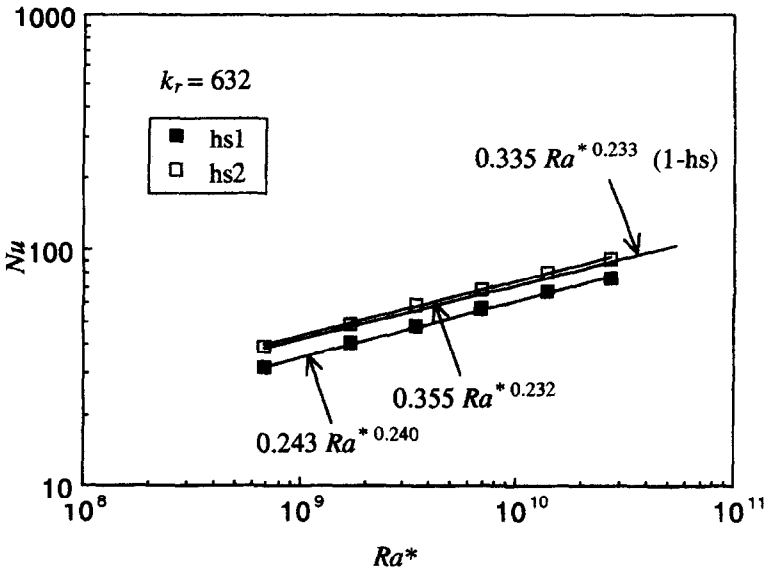

Fig. 11. Variation of Nu of the heat sources with Ra^* for $k_r = 632$ (two heat source configuration).

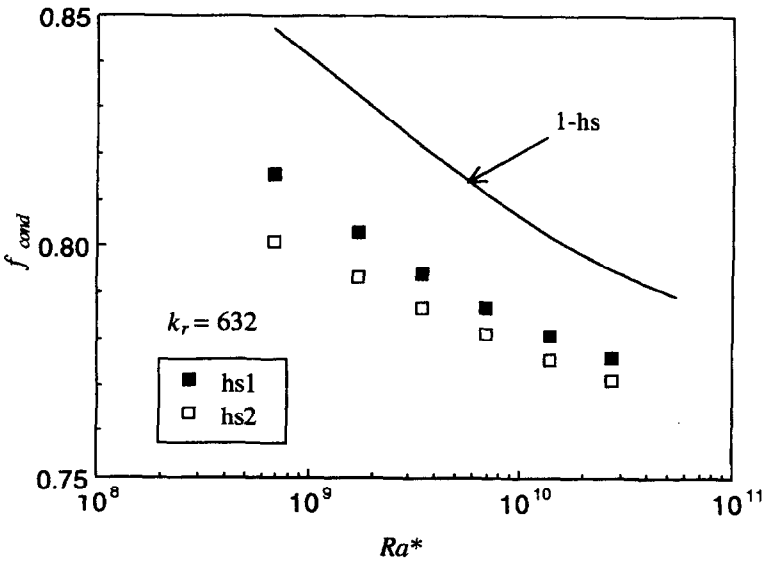

Fig. 12. Variation of conduction ratio (f_{cond}) vs Ra^* for $k_r = 632$ (two heat source configuration).

with increasing Ra^*. The hs2 has the advantage of having a cool upstream section of the vertical wall ($4.25 < X < 5$), while the upstream wall section of hs1 is warmed by thermal wake from hs2. This explains larger Nu for hs2. The result for the case of 1-hs, shown by a curve in Fig. 10, is again identical with the result for hs2, indicating the negligible influence of hs1 on heat transfer from hs2 due to relatively low thermal conductivity of the substrate. In the range of Ra^* studied, convection heat transfer from the substrate has a large contribution in cooling of both heat sources.

Figure 11 shows correlations of Nu vs Ra^* for $k_r = 632$. In this case the temperature of both heat sources were higher, and their dependence on Ra^* was stronger, than for the single heat source configuration (1-hs). On a highly conductive substrate, hs2 'sees' hs1 by means of the conduction through the wall, while on a low conductivity material, as seen in the results for $k_r = 24.6$, hs1 has negligible influence on hs2 as long as their separation distance is more than twice the size of the heat source. Furthermore, in a highly conductive substrate, hs2 'feels' the presence of the bottom adiabatic boundary. The combination of these effects causes an increase in the temperature of hs2 compared to the temperature in the single heat source configuration. The higher temperature of hs2 leads to a slightly higher Nu compared with the single heat source configuration (Fig. 11). Further, the hs1 temperature is higher than hs2 whereas the Nusselt number of hs2 is higher. Comparing the temperature

of both hs1 and hs2, it is seen that the temperature of hs1 is higher and its Nu is lower than hs2. This is attributed to both the thermal wake effect and thermal influence of hs2 by conduction through the wall.

The ratio of heat conduction in the wall to the source heat dissipation is shown in Fig. 12 for $k_r = 632$. For comparing the single heat source configuration values are also presented. It is seen that f_{cond} decreases with increasing Ra^* for both heat sources as expected. On this highly conductive substrate more than 75% of the generated heat is conducted to the plate, with a substantial part of this being convected to the coolant in the adjacent channel. From comparison of the average Nus on both front and back faces of the wall, it is found that heat transfer rates on both faces are nearly equal. This coincides with a symmetric flow pattern described earlier.

The following phenomena in conjugate heat transfer from highly conductive substrates can be observed in Fig. 12. First, f_{cond} for both hs1 and hs2 is lower than that of the 1-hs configuration. The wall acts as a heat spreader in both configurations. Heat spreading is bound by the adiabatic top and bottom boundaries, and more so when there are multiple heat sources. Also, in the case of two heat sources, there is a smaller surface area of the wall available for convecting the heat conduction to the wall. These thermal and geometric constrains on heat transfer explain the relatively low ratios of heat conduction in the 2-hs configuration. Second, f_{cond} of hs1 is higher than that of hs2, in contrast to the result shown in Fig. 10 for the case of low thermal conductivity substrate. In the high conductivity substrate heat spreading from hs2 is bound by the presence of hs1 and the adiabatic bottom, namely, hs2 is in a thermally more restrictive environment than hs1. The hs1 is covered by thermal wake from hs2, which proves detrimental for heat transfer from hs1 on the low conductivity substrate, however, has a wider area for heat spreading than hs2. The effect of wide heat spreading from hs1, which results from the location of hs1 at the mid-height of the wall, offsets the negative effect of thermal wake from below.

4. CONCLUSIONS

A parametric study on natural convection immersion cooling of multiple heat sources in parallel interacting cavities filled with FC-72 has clarified the influence of Ra^* and k_r on the flow and thermal fields, and the heat transfer characteristics of the heat generating devices. Increasing Ra^* leads to a stronger convective flow inside the cavities for all values of k_r. Thin thermal and velocity boundary layers are formed along both faces of the vertical walls and the rest of the cavity is occupied by the cold fluid. For low values of k_r (e.g. bakelite substrate), the flow and thermal fields are asymmetric whilst for higher conductivity substrates (e.g. alumina–ceramic), symmetrical flow patterns are observed.

The non-dimensional heat source temperatures and Nusselt numbers are well correlated with Ra^* for different wall materials and compared with the base case analysis of single heat source conditions. For the base case analysis, the exponent of the correlations for the non-dimensional temperature is -0.163 ± 0.004 for $24.6 \leqslant k_r \leqslant 632$. For the cavities with $k_r = 24.6$, the heat transfer performance of hs2 is independent of hs1 due to the high thermal resistance in the wall. However, hs2 has an influence on hs1 via its thermal wake. For $k_r = 632$, both heat sources are thermally coupled by heat conduction in the substrate. This results in a higher temperature for both heat sources when compared to the single heat source configuration. The temperature of hs1 is found to be higher than the temperature of hs2 for all values of k_r. For $k_r = 24.6$, the convection is the major cooling mode whilst for $k_r = 632$, conduction to the substrate is significant.

REFERENCES

1. Johnson, C. E., Evaluation of correlations for natural convection cooling of electronic equipment. *Heat Transfer in Electronic Equipment*, 1986, ASME HTD- **57**, 103–111.
2. Bergles, A. E. and Bar-Cohen, A., Direct liquid cooling of microelectronic components. *Advances in Thermal Modeling of Electronic Components and Systems*, eds. A. Bar-Cohen and A. D. Kraus, Vol. 2, 1990, pp. 233–342.
3. Milanez, L. F. and Bergles, A. E., Studies on natural convection heat transfer from thermal sources on a vertical surface. *Proceedings of Eighth International Heat Transfer Conference*, 1986, pp. 1347–1352.
4. Jaluria, Y., Buoyancy-induced flow due to isolated thermal sources on a vertical surface. *ASME Journal of Heat Transfer*, 1982, **104**, 223–227.
5. Park, K. A. and Bergles, A. E., Natural convection heat transfer characteristics of simulated microelectronic chips. *ASME Journal of Heat Transfer*, 1987, **109**, 90–96.
6. Fujii, T. and Fujii, M., The dependence of local Nusselt number on Prandtl number in the case of free convection along a vertical surface with uniform heat flux. *International Journal of Heat and Mass Transfer*, 1976, **19**, 121–122.
7. Keyhani, M., Prasad, V. and Cox, R., An experimental study of natural convection in a vertical cavity with discrete heat sources. *ASME Journal of Heat Transfer*, 1988, **110**, 616–624.
8. Keyhani, M., Prasad, V., Shen, R. and Wong, T. T., Free convection heat transfer from discrete heat sources in a vertical cavity. *Natural and Mixed Convection in Electronic Equipment Cooling*, ed. R. A. Writz, ASME HTD 1988, **100**, 13–24.
9. Shen, R., Prasad, V. and Keyhani, M., Effect of aspect ratio and size of heat source on free convection in a discretely heated vertical cavity. In *Numerical Simulation of Convection in Electronic Equipment Cooling*, ASME HTD-Vol. 121, 1989, pp. 45–54.
10. Sathe, S. B. and Joshi, Y., Natural convection arising from a heat generating substrate-mounted protrusion in a liquid-filled two-dimensional enclosure. *International Journal of Heat Mass Transfer*, 1991, **14**(8), 2149–2163.
11. Joshi, Y. and Paje, R. A., Natural convection cooling of a ceramic substrate mounted leadless chip carrier in dielectric liquids. *International Communication of Heat and Mass Transfer*, 1991, **18**, 39–47.
12. Sathe, S. B. and Joshi, Y., Natural convection liquid

cooling of a substrate-mounted protrusion in a square enclosure: a parametric study. *ASME Journal of Heat Transfer*, 1992, **114,** 401–409.
13. Wroblewski, D. and Joshi, Y., Computations of liquid immersion cooling for a protruding heat source in a cubical enclosure. *International Journal of Heat and Mass Transfer*, 1993, **36**(5), 1201–1218.
14. Wroblewski, D. and Joshi, Y., Liquid immersion cooling of a substrate-mounted protrusion in a three-dimensional enclosure: the effects of geometry and boundary conditions. *ASME Journal of Heat Transfer*, 1994, **116,** 112–119.
15. Wroblewski, D. and Joshi, Y., Transient natural convection from a leadless chip carrier in a liquid filled enclosure: a numerical study. *ASME Journal of Electronic Packaging*, 1992, **114,** 271–279.
16. Kim, S. H., Anand, N. K. and Aung, W., Effect of wall conduction on free convection between asymmetrically heated vertical plates: uniform wall heat flux. *International Journal of Heat and Mass Transfer*, 1990, **33**(5), 1013–1023.
17. Jaluria, Y., Interaction of natural convection wakes arising from thermal sources on a vertical surface. *ASME Journal of Heat Transfer*, 1985, **107,** 883–892.
18. Gosman, A. D., Lockwood, F. C. and Tatchell, G., A numerical study of the heat-transfer performance of the open thermosyphon. *International Journal of Heat and Mass Transfer*, 1971, **14,** 1717–1730.
19. Chan, Y. L. and Tien, C. L., A numerical study of two-dimensional laminar natural convection in shallow open cavities. *International Journal of Heat and Mass Transfer*, 1985b, **28,** 603–612.
20. Abib, A. H. and Jaluria, Y., Numerical simulation of the buoyancy induced flow in a partially open enclosure. *Numerical Heat Transfer*, 1988, **14,** 235–254.
21. Lage, J. L., Lim, J. S. and Bejan, A., Natural convection with radiation in a cavity with open top end. *ASME Journal of Heat Transfer*, 1992, **114,** 479–486.
22. Jones, G. F. and Cai, J., Analysis of a transient asymmetrically heated/cooled open thermosyphon. *ASME Journal of Heat Transfer*, 1993, **115,** 621–630.
23. Patankar, S. V., Numerical Heat Transfer and Fluid Flow. Hemisphere, Washington, D.C., 1980.
24. Samarskii, A. A. and Andreyev, V. B., On a high-accuracy difference scheme for an elliptic equation with several space variables. *USSR Computational Mathematics and Physics*, 1963, **3,** 1373–1382.
25. Heindel, T. J., Ramadhyani, S. and Incropera, F. P., Liquid immersion cooling of a longitudinal array of discrete heat sources in protruding substrates: II—forced convection boiling. *ASME Journal of Electronic Packaging*, 1992, **114,** 63–70.
26. Dehgham, A. A. and Behnia, M., Combined natural convection–conduction and radiation heat transfer in a discretely heated open cavity. *ASME Journal of Heat Transfer*, 1996, **118,** 56–64.